Final Draft
of the original manuscript:

Gussone, J.; Garces, G.; Haubrich, J.; Stark, A.; Hagedorn, Y.-C.; Schell, N.; Requena, G.:

Microstructure stability of Gamma-TiAl produced by selective laser melting

In: Scripta Materialia (2016) Elsevier

DOI: 10.1016/j.scriptamat.2016.11.028

Microstructure stability of γ-TiAl produced by selective laser melting

J. Gussone[1], G. Garces[2], J. Haubrich[1], A. Stark[3], Y. Hagedorn[4], N. Schell[3], G. Requena[1,5]

[1] Department of Metals and Hybrid Materials, Institute of Materials Research, German Aerospace Center, Linder Höhe, 51147, Cologne, Germany

[2] Department of Physical Metallurgy, National Center for Metallurgical Research (CENIM-CSIC), Avda. Gregorio del Amo 8, 28040 Madrid, Spain

[3] Institute of Materials Research, Helmholtz-Zentrum Geesthacht, Max-Planck-Str. 1, 21502 Geesthacht, Germany

[4] Fraunhofer Institute for Laser Technology, Steinbachstraße 15, 52074 Aachen, Germany

[5] RWTH Aachen, 52062Aachen, Germany

Abstract:

The effects of intrinsic heat-treatment during SLM processing of a TiAl alloy are studied and compared to extrinsic post-annealing. Phase evolution during heat-treatment of as-built Ti-44.8Al-6Nb-1.0Mo-0.1B studied by in situ synchrotron diffraction showed pronounced intensity changes and peak shifts for α_2 below the eutectoid temperature, which are explained by stabilization of supersaturated α_2 as well as transformations to γ and β/B2.These observations are in contrast to marginal intensity changes found for the microstructure thermodynamically stabilized by HIP. The intrinsic heat-treatment of the as-built state leads to graded microstructures characterized by an increase of globular γ and β/B2 at the α_2/γ colony boundaries.

γ-TiAl alloys are well-suited for aerospace applications due to their low density, high temperature strength and Young's modulus as well as very good corrosion and oxidation resistance [1]. Their technological maturity has been proven by recent applications, e.g. as cast turbine blades made of the Ti-48Al-2Cr-2Nb alloy were introduced in the last two rotor

stages of the low pressure turbine of the GEnX jet engine [2]. However, current products are restricted to conventional processing routes, i.e. casting and forging. The development of suitable processing conditions for additive layer manufacturing (ALM) of γ-TiAl alloys would allow the realisation of more complex geometries, e.g. components with cooling channels and hollow structures, as well as the reduction of lead time and material savings. Although most research activities regarding ALM of TiAl alloys currently deal with electron beam melting (EBM) [3-6], a few studies also demonstrate that TiAl alloys can be processed by selective laser melting (SLM) [7-11].

However, additive manufacturing of γ-TiAl is still very demanding: (i) the fast cooling rates typical of ALM induce residual stresses that lead to crack formation and (ii) evaporation of Al in molten condition results in compositional variations of the alloy. These two effects must be overcome to avoid deficient products (LMD [10], EBM [4], SLM [10]). One promising approach to reduce residual stresses is to increase the temperature of the substrate plate sufficiently during ALM followed by slow cooling after completion of the process [8, 11]. This reduces the temperature gradient between the solidifying layers and the lower parts of the built specimens and thus decreases the magnitude of the thermal stresses. Furthermore, if the temperature is high enough, these thermal stresses can be at least partially relaxed during processing and slow cooling.

Another fact that must be taken into account during ALM of γ-TiAl alloys is that the microstructures formed are usually far from thermodynamic equilibrium conditions. Fast solidification and cooling rates, for instance, can result in the formation of metastable phases and, therefore, microstructural changes can occur during subsequent exposure to high temperatures. Moreover, the heating of solidified layers as new powder layers are successively deposited and molten (termed here as intrinsic heat treatment), can result in the formation of a graded microstructure in the building direction.

The microstructural stability of conventionally produced γ-TiAl alloys and its impact on mechanical behaviour has been examined in a few studies that include in situ experiments to follow microstructural evolution during heat treatment (e.g. [12-15]). These investigations mainly focus on the development of the microstructure from supersaturated α_2 obtained by quenching and aging below the eutectoid temperature [12, 13, 16, 17]. The importance of these processes for powder metallurgy and additive manufacturing was recently pointed out considering that the fast cooling rates during ALM can be to some extent compared to quenching from temperatures above the eutectoid temperature [18]. Nevertheless, it should be taken into account that cooling rates during SLM can be orders of magnitude higher than during quenching [19].

SLM as-built microstructures are the result of a more complex thermal history, i.e. short remelting of the upper layers of deposited material and heating cycles with decreasing temperature take place as the SLM process advances [20-22]. The intrinsic heat treatment gradually converges to an isothermal heat treatment at the baseplate temperature as the number of layers built increases, likely leading to a vertical gradient of the materials' properties besides the already known anisotropy due to the layer-wise building process. Since the present phases and their morphology form the basis of the materials' properties, it is necessary to characterize SLM as-built microstructures in terms of phases formed, their distribution along the building direction and their stability during high temperature exposure.

For this purpose Ti-44.8Al-6Nb-1.0Mo-0.1B (at.-%) - an alloy under development for turbine blade application - was manufactured by SLM at the Fraunhofer Institute for Laser Technology, Aachen, using a laboratory SLM machine. The baseplate was held at 800°C during manufacturing of samples with a size of 10×10×5 mm^3. An energy density of 60 J/mm^3 was applied as a result of the combination of laser power = XXX, scan velocity = XXX , hatch distance = XXX and layer thickness = XXX [Energy density]. The microstructure of the

SLM samples and their thermal stability was studied for two initial conditions, i.e. as-built and after hot isostatic pressing (HIP). HIP was carried out at 1200 °C with an applied stress of 200 MPa for 4h and subsequent cooling at 10 K/min down to room temperature. The HIP treatment is expected to render a thermodynamically more stable microstructure. The initial microstructure of the as-built and HIP samples was studied by SEM and TEM. The thermal stability of the two conditions was studied at about 4-5 mm from the upper surface by *in situ* high energy X-ray diffraction (HEXRD) during heating. The experiments were carried out at the beamline P07 of the synchrotron source Petra III at DESY, Hamburg. A monochromatic beam with an energy of 100 keV was used for HEXRD in transmission mode (sample thickness = ca.4 mm) with a slit size of 1×1 mm^2. A modified dilatometer Bähr 805A/D with an induction coil furnace was used to heat the samples at 20 K/min up to 1200°C in a high purity argon atmosphere (> 99.999%). 2D diffraction patterns were collected during heating using a Perkin Elmer flat panel detector (XRD 1621) at an acquisition rate of ~ 1 image / 10 s. The samples were kept fixed during acquisition and the temperature was controlled by a B-type thermocouple spot-welded next to the position of the incoming beam. Azimuthal integration of the Debye-Scherrer rings from the bulk of the samples was carried out using the software fit2D [23]. Additionally, the variation of the diffraction reflexes along the building direction (z-direction) was investigated for the as-built condition along the sample height of 5 mm to examine the microstructural gradient induced by the intrinsic heat treatment.

Different microstructures can be expected for conventionally produced γ-TiAl alloys depending on the annealing temperature and the cooling rate. Microstructures with combinations of lamellar, Widmanstätten, feathery lamellar, massive gamma and supersaturated α_2 structures have been found for a large variety of TiAl alloys quenched from the α-field [24]. The SLM as-built microstructure can be described as a very fine near lamellar microstructure (Figure 1a) with sub-µm-sized equiaxed γ-TiAl (dark) and β/B2 (bright) grains decorating the α_2/γ colony boundaries. TEM reveals that the lamellar colonies

partially exhibit order domains with phase/antiphase boundaries (Figure 1b) [25, 26]. Despite the high cooling rates, and in contrast to quenched γ-TiAl [27, 28], the γ-laths formation within the supersaturated α_2-Ti_3Al is not fully suppressed due to the combined effect of the intrinsic heat treatment and the preheat temperature of 800°C during the SLM process. The SLM+HIP condition leads to mainly globular microstructure (Figure 1c, d) with a few regions appearing to have originated from the former α_2/γ lamellar structure (cp. Figure 1d).

A comparison of HEXRD patterns obtained at RT shows broader diffraction peaks for the SLM as-built condition than for SLM+HIP (Figure 2a) due to the fine thickness of the α_2/γ lamellae and high coherence strains [29]. Furthermore, the γ-(002) and γ-(200) reflexes appear as a single peak for the as-built condition indicating a small tetragonality. In contrast, at 1175°C (Figure 2b), which is sufficiently below the eutectoid temperature of the alloy ($T_{eutectoid}$ ≈1200°C [30]), the diffraction patterns of as-built and HIP conditions do not show these differences anymore.

The evolution of both conditions (SLM and SLM+HIP) during heating is shown by the colour coded 2D representation of the reflex intensities during heating from 700 °C to ~ 1200 °C in Figure 3 for a 2θ-range between 2.4 and 3.6°. In the case of the HIP condition, comparatively small intensity changes beginning at around 1050°C can be observed: an increase for the β/B2-(110) and β/B2-(100) reflexes, a decrease for α_2, especially α_2 -(101), a decrease of γ-(200) and an increase of α_2-(200). On the other hand, the initially broad reflexes of the as-built condition become narrower above ~ 900 °C. This may be a result of diffusion-induced relaxation of coherence strains at the α_2/γ interfaces and re-ordering of the phase/antiphase boundaries and coarsening of the α_2/γ colonies.

Significant changes are shown during heating by the α_2-reflexes in the as-built condition. Between ca. 800 and 950°C there is a decrease in intensity while it increases again significantly at T > 950°C. Furthermore, peak shifts take place between ca 900 and 1000°C. Interestingly, these shifts are more pronounced for α_2-(100) and α_2-(200) / α-(100), whereas

the α_2-(101) reflex mainly shows an increase of the peak intensity. Simultaneously, the intensity of the γ-(200) reflex begins to increase strongly at ~ 950°C and reaches a maximum at ~ 1050°C, consistent with the formation and growth of γ-laths from supersaturated-α_2. The formation of α_2/γ lamellae was also observed with TEM in situ during heat treatment at 730°C for oil-quenched Ti-45Al-7.5Nb with an initial microstructure consisting of supersaturated-α_2 with massive γ at α_2 grain boundaries and, especially, at triple points [12, 31]. The changes of the α_2 and γ reflexes between 800°C and 1000°C for the as-built condition suggest that metastable supersaturated-α_2 was formed during SLM and is still retained, especially in upper layers of material. As diffusion is activated during heating, the metastable supersaturated-α_2 decomposes into α_2+γ. This decomposition is accompanied by element partition, particularly Al atoms that diffuse from supersaturated-α_2 into γ (*supersaturated-α_2 → α_2+γ)*. Thus, the peak shift observed is a result of the changes in the chemical composition between supersaturated-α_2 and α_2 [32], while the decreases and increases in the intensity of α_2/γ reflexes indicate a dissolution and formation of these phases, respectively. At T > 1050°C the γ-(200) peak intensity decreases again together with the increase of β/B2 and α_2, similarly to the HIP condition. Small variations of the peak intensities can also be found along the SLM building direction in the as-built condition (Figure 4a), due to a graded microstructure as a result of the intrinsic heat treatment. An increase of the intensities of β/B2 and γ reflexes is observed simultaneously with a decrease for α_2-(200) as the distance from the last deposited powder layer increases. No pronounced peak shifts of α_2 reflexes could be observed as a function of z. SEM images from the corresponding z-positions show an increase of globular β/B2 and γ at the colony boundaries (Figure 4b). During the intrinsic heat treatment α_2 transforms to γ (transferring Al) and β/B2 (transferring Nb, Mo). Due to a high coherence of the γ/ α_2 phase boundaries β/B2 generally does not precipitate within the colonies, and full stabilization of α_2 does not take place as the temperature is too low for long range diffusion processes.

In summary, using HEXRD we show that significant microstructural transformations are induced by heating the as-built alloy Ti-44.8Al-6Nb-1.0Mo-0.1B up to 1200°C, which differs strongly from the corresponding annealing experiment of a material that was more stabilized and closer to thermodynamic equilibrium due to HIP at 1200°C. Moreover, we show that the intrinsic heat treatment during the SLM process leads to phase evolutions consistent with the post-annealing below 950°C. Our ongoing studies will focus next on the origin and development of the domains within the α_2/γ-colonies, the evolution of the microstructure and the chemical composition of the phases depending on the intrinsic heat treatment conditions.

Acknowledgements

The authors gratefully acknowledge the beam-time allocation for proposal XXX at beamline P07 of the synchrotron source Petra III at DESY, Hamburg.

References

1. Clemens, H., et al., *Design of Novel β-Solidifying TiAl Alloys with Adjustable β/B2-Phase Fraction and Excellent Hot-Workability.* Advanced Engineering Materials, 2008. **10**(8): p. 707-713.
2. Clark, S.F. *787 Propulsion System*. Aero Quarterly; Available from: http://www.boeing.com/commercial/aeromagazine/articles/2012_q3/2/.
3. Baudana, G., et al., *Electron Beam Melting of Ti-48Al-2Nb-0.7Cr-0.3Si: Feasibility investigation.* Intermetallics, 2016. **73**: p. 43-49.
4. Schwerdtfeger, J. and C. Körner, *Selective electron beam melting of Ti–48Al–2Nb–2Cr: Microstructure and aluminium loss.* Intermetallics, 2014. **49**(0): p. 29-35.
5. Biamino, S., et al., *Electron beam melting of Ti–48Al–2Cr–2Nb alloy: Microstructure and mechanical properties investigation.* Intermetallics, 2011. **19**(6): p. 776-781.
6. Murr, L.E., et al., *Characterization of titanium aluminide alloy components fabricated by additive manufacturing using electron beam melting.* Acta Materialia, 2010. **58**(5): p. 1887-1894.
7. Löber, L., et al., *Selective laser melting of a beta-solidifying TNM-B1 titanium aluminide alloy.* Journal of Materials Processing Technology, 2014. **214**(9): p. 1852-1860.
8. Gussone, J., et al., *Microstructure of γ-titanium aluminide processed by selective laser melting at elevated temperatures.* Intermetallics, 2015. **66**: p. 133-140.
9. Li, W., et al., *Effect of laser scanning speed on a Ti-45Al-2Cr-5Nb alloy processed by selective laser melting: Microstructure, phase and mechanical properties.* Journal of Alloys and Compounds, 2016. **688**: p. 626–636.
10. Vilaro, T., et al., *Direct Fabrication of a Ti-47Al-2Cr-2Nb Alloy by Selective Laser Melting and Direct Metal Deposition Processes.* Advanced Materials Research, 2010. **89-91**: p. 586-591.
11. Li, W., et al., *Effect of substrate preheating on the texture, phase and nanohardness of a Ti–45Al–2Cr–5Nb alloy processed by selective laser melting.* Scripta Materialia, 2016. **118**: p. 13-18.

12. Cha, L., et al., *In Situ Study of γ-TiAl Lamellae Formation in Supersaturated α2-Ti3Al Grains.* Advanced Engineering Materials, 2012. **14**(5): p. 299-303.
13. Liss, K.-D., et al. *IN-SITU CHARACTERIZATION OF PHASE TRANSFORMATIONS AND MICROSTRUCTURE EVOLUTION IN A γ-TiAl BASED ALLOY* in *TMS 2008 annual meeting & exhibition*. 2008. New Orleans, Louisiana, USA.
14. Liss, K.D., et al., *Directional Atomic Rearrangements During Transformations Between the α- and γ-Phases in Titanium Aluminides.* Advanced Engineering Materials, 2008. **10**(4): p. 389-392.
15. San Juan, J., et al., *Atomic relaxation processes in an intermetallic Ti–43Al–4Nb–1Mo–0.1B alloy studied by mechanical spectroscopy.* Acta Materialia, 2014. **65**: p. 338-350.
16. Erdely, P., et al., *In Situ Characterization Techniques Based on Synchrotron Radiation and Neutrons Applied for the Development of an Engineering Intermetallic Titanium Aluminide Alloy.* Metals, 2016. **6**(1): p. 10.
17. Sun, Y.Q., *Nanometer-scale, fully lamellar microstructure in an aged TiAl-based alloy.* Metallurgical and Materials Transactions A: Physical Metallurgy and Materials Science, 1998. **29**(11): p. 2679-2685.
18. Guyon, J., A. Hazotte, and E. Bouzy, *Evolution of metastable α phase during heating of Ti48Al2Cr2Nb intermetallic alloy.* Journal of Alloys and Compounds, 2016. **656**: p. 667-675.
19. Yang, J., et al., *Formation and control of martensite in Ti-6Al-4V alloy produced by selective laser melting.* Materials & Design, 2016. **108**: p. 308-318.
20. Martukanitz, R., et al., *Toward an integrated computational system for describing the additive manufacturing process for metallic materials.* Additive Manufacturing, 2014. **1–4**: p. 52-63.
21. Hodge, N.E., R.M. Ferencz, and J.M. Solberg, *Implementation of a thermomechanical model for the simulation of selective laser melting.* Computational Mechanics, 2014. **54**(1): p. 33-51.
22. Fu, C.H. and Y.B. Guo, *Three-Dimensional Temperature Gradient Mechanism in Selective Laser Melting of Ti-6Al-4V.* Journal of Manufacturing Science and Engineering, 2014. **136**(6): p. 061004-061004.
23. ; Available from: http://www.esrf.eu/computing/scientific/FIT2D/.
24. Hu, D., A.J. Huang, and X. Wu, *On the massive phase transformation regime in TiAl alloys: The alloying effect on massive/lamellar competition.* Intermetallics, 2007. **15**(3): p. 327-332.
25. Denquin, A. and S. Naka, *Phase transformation mechanisms involved in two-phase TiAl-based alloys—II. Discontinuous coarsening and massive-type transformation.* Acta Materialia, 1996. **44**(1): p. 353-365.
26. Denquin, A. and S. Naka, *Phase transformation mechanisms involved in two-phase TiAl-based alloys—I. Lambellar structure formation.* Acta Materialia, 1996. **44**(1): p. 343-352.
27. Gamsjäger, E., et al., *Diffusive and massive phase transformations in Ti–Al–Nb alloys – Modelling and experiments.* Intermetallics, 2013. **38**: p. 126-138.
28. Cha, L., H. Clemens, and G. Dehm, *Microstructure evolution and mechanical properties of an intermetallic Ti-43.5Al-4Nb-1Mo-0.1B alloy after ageing below the eutectoid temperature.* International Journal of Materials Research, 2011. **102**(6): p. 703-708.
29. Schmoelzer, T., et al., *The Contribution of High-Energy X-Rays and Neutrons to Characterization and Development of Intermetallic Titanium Aluminides.* Advanced Engineering Materials, 2011. **13**(8): p. 685-699.
30. Bolz, S., et al., *Microstructure and mechanical properties of a forged β-solidifying γ TiAl alloy in different heat treatment conditions.* Intermetallics, 2015. **58**(0): p. 71-83.
31. Cha, L., et al., *Nanometer-scaled lamellar microstructures in Ti–45Al–7.5Nb–(0; 0.5)C alloys and their influence on hardness.* Intermetallics, 2008. **16**(7): p. 868-875.
32. Appel, F., *Phase Transformations and Recrystallization Processes During Synthesis, Processing and Service of TiAl Alloys*, in *Recrystallization*, K. Sztwiertnia, Editor 2012, InTech. p. 225-266.

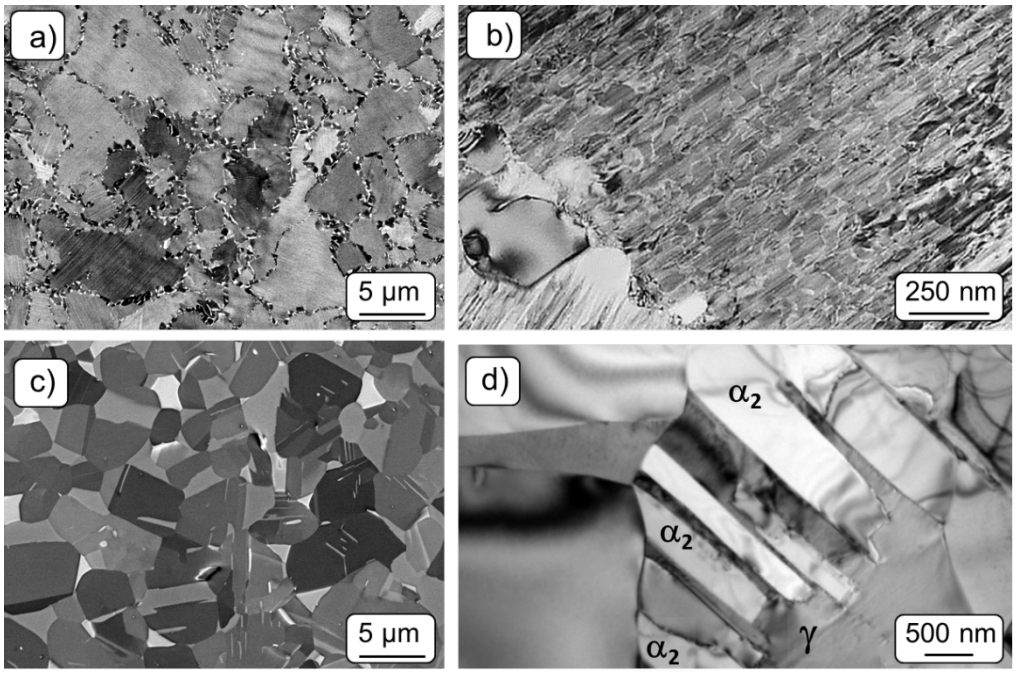

Figure 1: As- built (a, b) and SLM+HIP (c, d) microstructures from the centre of Ti-44.8Al-6Nb-1.0Mo-0.1B alloy manufactured with SLM at 800 °C. SEM image (a) showing very fine irregular near-lamellar structure (γ and β/B2 at α_2/γ colony boundaries). A corresponding TEM image (b) shows lamellar colonies with adjacent globular grains. Some colonies exhibit domains separated by phase / antiphase boundaries. SEM image (c) of the SLM+HIP condition showing a globular structure with areas showing relicts from the lamellar colonies. One of these areas is shown in a TEM image (d).

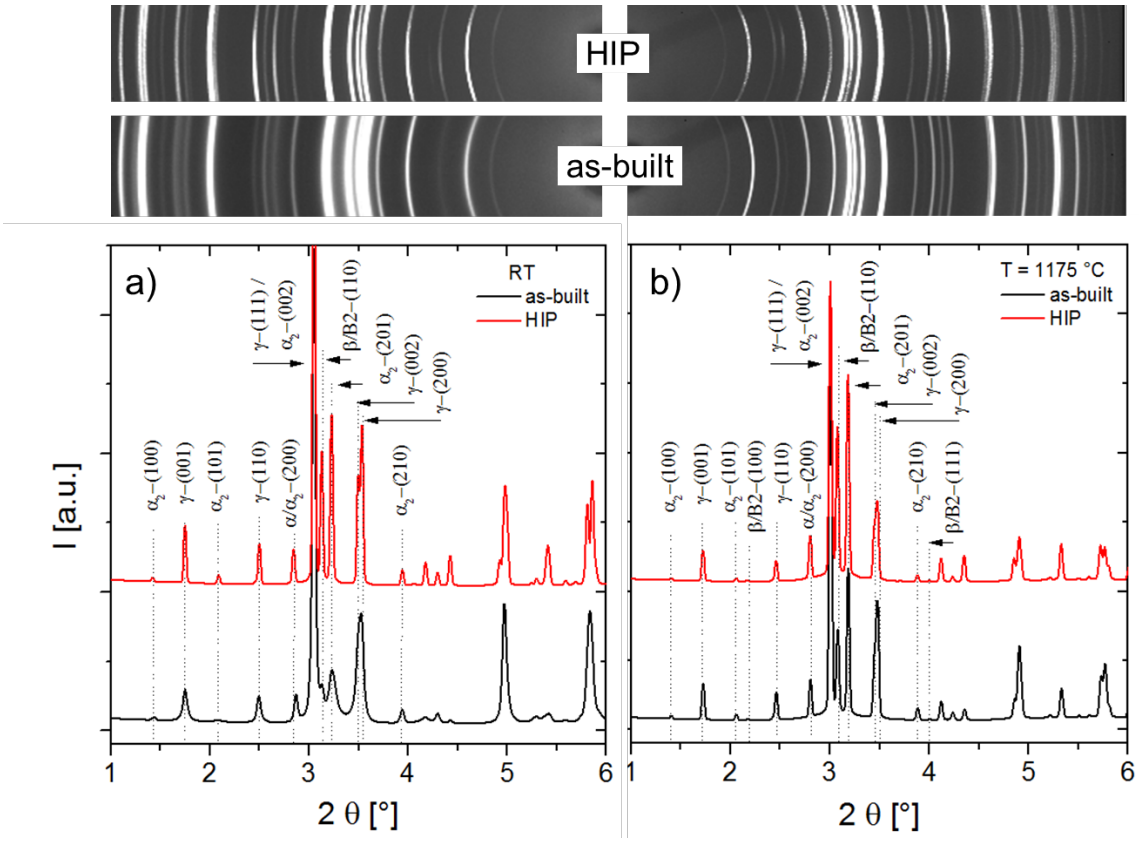

Figure 2: Comparison of diffractograms (SLM and SLM+HIP) before the heat treatment (a) and at 1175°C (b).

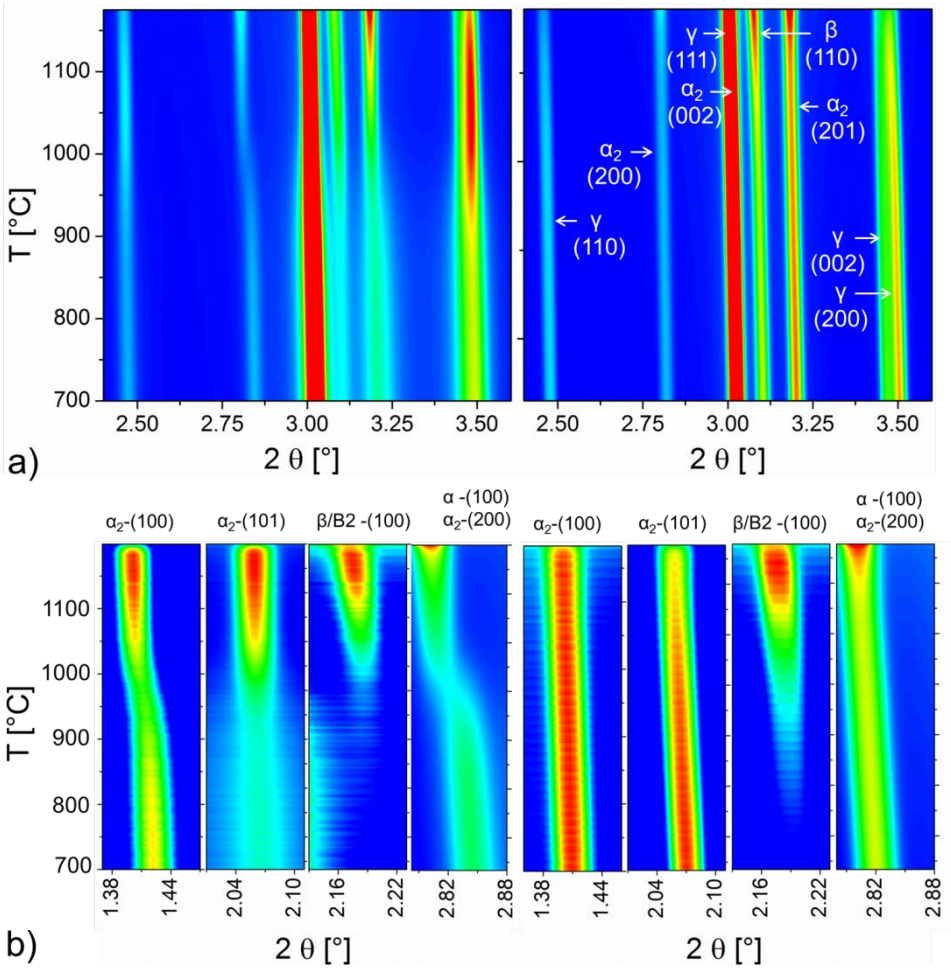

Figure 3: Evolution of reflections during heating from 700°C to 1200°C with a constant heating rate of 20K/min. a) Comparison of as-built condition (left) and after HIP at 1200°C (right). b) Development of selected superlattice peaks as-built (left) and HIP (right).

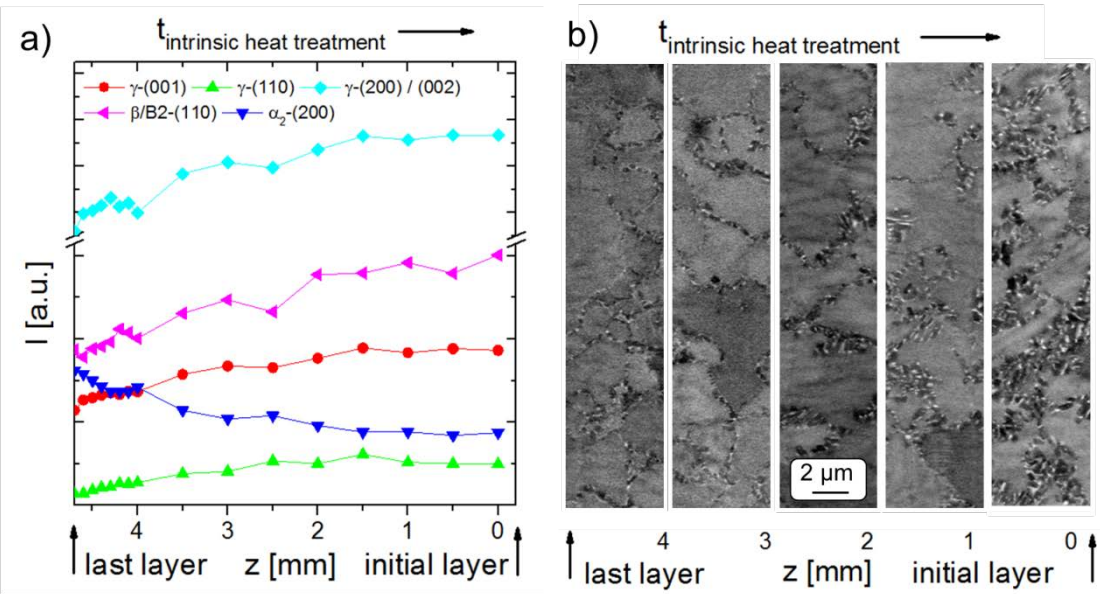

Figure 4: Intensity of selected XRD reflections (a). The z-position corresponds to the sample height (build direction). The position close to the baseplate (z = 0 mm) corresponds to the condition with the longest in situ-heat treatment (ca. 3 h). For this measurement the beam size was reduced to 0.1×0.5 mm^2 (z, x). SEM images of graded microstructure from corresponding z-positions (b).